Digital access to libraries

"The influence of microstructure and composition on the plastic behaviour of dual-phase steels"

Pierman, Anne-Pascale ; Bouaziz, O. ; Pardoen, Thomas ; Jacques, Pascal ; Brassart, Laurence

Abstract

This paper presents a systematic experimental study of the relative contributions of the martensite volume fraction, morphology and carbon content to the overall strength and ductility of dual-phase steels. To this end, model dual-phase steels combining three volume fractions of martensite, three martensitic carbon contents, and three arrangements of the phases were generated by suitable control of the heat treatments. The microstructures include long and short elongated, as well as equiaxed martensitic islands. The yield and tensile strengths increase with both the amount of martensite and its carbon content. The ductility in general increases with the volume fraction of martensite at constant martensitic carbon content, and conversely increases with the martensitic carbon content for a fixed volume fraction of martensite. Departure from the general trend is observed for combinations of a large volume fraction of martensite with a large martensitic carbon content, and is attributed ...

Document type : *Article de périodique (Journal article)*

Référence bibliographique

The influence of microstructure and composition on the plastic behaviour of dual-phase steels

A.-P. Pierman [a], O. Bouaziz [b], T. Pardoen [a], P.J. Jacques [a], L. Brassart [a,*]

[a] *Institute of Mechanics, Materials and Civil Engineering, Université catholique de Louvain, 2 Pl. Sainte-Barbe, Bâtiment Réaumur, B-1348 Louvain-la-Neuve, Belgium*
[b] *Laboratoire d'Etude des Microstructures et de Mécanique des Matériaux (LEM3), CNRS UMR 7239, Université de Lorraine, Metz, France*

Abstract

This paper presents a systematic experimental study of the relative contributions of the martensite volume fraction, morphology and carbon content to the overall strength and ductility of dual-phase steels. To this end, model dual-phase steels combining three volume fractions of martensite, three martensitic carbon contents, and three arrangements of the phases were generated by suitable control of the heat treatments. The microstructures include long and short elongated, as well as equiaxed martensitic islands. The yield and tensile strengths increase with both the amount of martensite and its carbon content. The ductility in general increases with the volume fraction of martensite at constant martensitic carbon content, and conversely increases with the martensitic carbon content for a fixed volume fraction of martensite. Departure from the general trend is observed for combinations of a large volume fraction of martensite with a large martensitic carbon content, and is attributed to damage-induced softening or fracture. Specimens with long elongated martensite demonstrate an improved ductility compared to other microstructures. The plastic flow properties were further investigated by relying on a non-linear homogenization model which explicitly accounts for the microscopic parameters. The micromechanical model captures reasonably well the tensile behaviour for the complete range of martensite carbon contents and volume fractions.

1. Introduction

Dual-phase (DP) steels are increasingly used in automotive applications because of their unique combination of high strength and good formability. Their attractive mechanical properties stem from the composite nature of the microstructure, consisting of a ductile ferrite (α) reinforced by hard martensite (α') particles [1]. Another advantage of DP steels is the absence of Lüders bands during plastic flow, leading to a smooth sheet surface without the need for additional skin-passes. DP steels are also relatively cheap, owing to the limited amounts of expensive alloying elements they contain and the ability to use traditional processing routes.

The complexity of the microstructure of DP steels and the number of parameters affecting the end-use properties make the design of these alloys challenging with respect to the requirements of specific structural applications. In particular, the volume fraction of martensite, morphology and carbon content all significantly affect the mechanical properties [2–6]. Recent research efforts have focused on combining experimental characterization techniques with advanced micromechanical models to unravel the complex structure–property relationship. For instance, the constitutive

* Corresponding author.
E-mail addresses: annepascale.pierman@gmail.com (A.-P. Pierman), olivier.bouaziz@univ-lorraine.fr (O. Bouaziz), thomas.pardoen@uclouvain.be (T. Pardoen), pascal.jacques@uclouvain.be (P.J. Jacques), laurence.brassart@uclouvain.be (L. Brassart).

response of these phases has been investigated by in situ high-energy X-ray diffraction [7,8] and in situ neutron diffraction [9,10] in combination with polycrystal models. Nanoindentation has been used to probe the local hardening of the phases as a function of the distance from the grain boundaries [11–13]. Recently, the stress–strain response of ferrite and martensite was measured from compression tests on nanopillars excised from DP steels [14,13]. On the other hand, various micromechanical models have been used to understand and predict the partitioning of strain and stress between the phases, including empirical mixture rules [15,16], Eshelby-based homogenization theories [17–21] and finite-element simulations on representative microstructures [22–28].

Despite intense research efforts, the relative influence of each one of the various parameters has not yet been quantitatively partitioned. Many of the previously mentioned studies and numerous others in the literature focused on one industrial grade of steel, which does not allow the effect of the individual parameters to be distinguished. Indeed, the volume fraction of martensite and its carbon content are intrinsically connected through the intercritical reheating temperature (and time) that fixes the ferrite–austenite thermodynamic equilibrium. The main novel objective of the present contribution is to decouple the effects of the martensite volume fraction, carbon content and morphology on the flow properties by considering model DP steels.

We have designed and optimized processing routes to produce model DP steels presenting three volume fractions of α' (15, 30 or 60% α') with an elongated morphology. These volume fractions are chosen to be close to the industrial microstructures containing from 10 to 80% martensite. Each volume fraction is generated with three levels of carbon content within the martensite (0.15, 0.3 and 0.6 wt.% C). Two additional materials with 60% of martensite and 0.15 wt.% C carbon with equiaxed and short elongated martensite particles were produced to study the effect of the morphology separately. Uniaxial tensile tests were performed for all the considered materials. Our experimental results demonstrate the significant impact of all the microstructure parameters considered.

The influence of the volume fraction and carbon content on the mechanical response was further investigated by means of a non-linear mean-field model. Partitioning of the stress and strain among each phase is computed based on a combination of the direct and inverse Mori–Tanaka models. The influence of carbon content is accounted for at the level of the martensite constitutive response. The latter was fitted on experimental measurements on bulk martensitic samples. The model suggests that development of plastic flow in the martensite with the associated limit on the level of stress that this phase can carry is a key element in understanding the experimental trends.

The paper is organized as follows. The experimental procedure and flow curves are presented in Section 2. The micromechanical model and the comparison between numerical results and experimental data are presented in Section 3. The results are discussed in Section 4, before concluding.

2. Experiments

2.1. Processing of model dual-phase steels

Five steel grades differing by their global carbon content were cast in order to cover a wide range of martensite volume fractions and carbon contents (see Table 1 for the complete compositions). These grades were provided by ArcelorMittal as roughed, hot-rolled plates. These plates presented microstructures composed of ferrite and pearlite. Some banding oriented in the rolling direction was present in the grades with the two lowest carbon contents (grades 1 and 2 in Table 1). No extra cold deformation was applied to allow for the machining of the plates into cylindrical uniaxial test specimens [29].

Nine model microstructures of DP steels combining three levels of α' volume fraction $V_{\alpha'}$ (15, 30 or 60%) with three levels of martensite carbon content $C_{\alpha'}$ (0.15, 0.3 or 0.6 wt.%) were processed from the hot-rolled plates following carefully designed two-step heat treatments (Fig. 1(a)). First, the specimens were held for 15 min at 1100 °C before water quenching to obtain 100% martensitic samples with a prior austenite grain size around 200 μm. In the second step, so-called Thomas fibre microstructures were generated from the martensite reversion during intercritical annealing [3]. The temperature and time of the second holding stage fixed the volume fraction of α' and its carbon content. Representative micrographs of the resulting microstructures are given in Figs. 2 (a)– (c). Heat treatment conditions and volume fractions of martensite are reported in Table 2 for each targeted model microstructure. This table shows that accurate control of both temperature and time of holding was necessary to reach the desired levels of α' volume fractions and C content. The volume fractions of α' in the different specimens were determined through a point counting procedure performed on scanning electron microscopy (SEM) micrographs after polishing and Nital etching. Neglecting the very small solubility of carbon in the ferrite (<0.02 wt.%), the C content in the martensite can be related to the total C content, C_{total}, by:

$$C_{\alpha'} = \frac{C_{total}}{V_{\alpha'}}. \tag{1}$$

The error in the estimated C content in the α' introduced by this approximation most probably falls within the margin of error on the measure of the α' volume fraction, which

Table 1
Chemical composition (wt.%) of the five steel grades investigated.

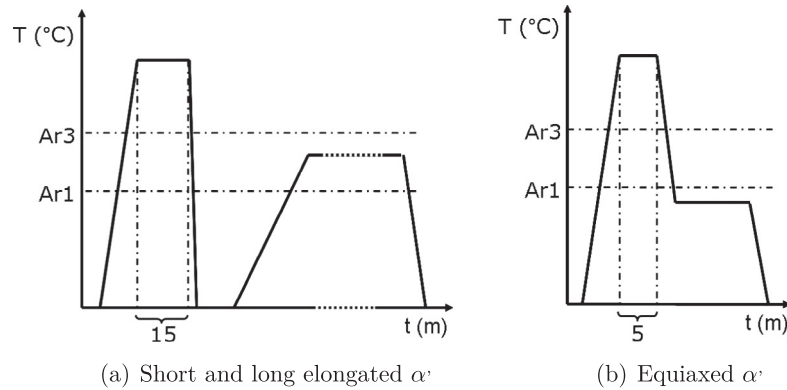| Grade	C	Si	Mn	P	S	Cr	Al
1	0.023	0.31	2.05	0.012	0.003	0.405	0.038
2	0.046	0.31	2.11	0.013	0.003	0.400	0.028
3	0.088	0.31	2.07	0.003	0.003	0.435	0.036
4	0.175	0.31	2.10	0.014	0.003	0.415	0.024
5	0.355	0.31	2.07	0.013	0.003	0.405	0.041

Fig. 1. Schematic representation of the heat treatments carried out to generate (a) short and long elongated and (b) equiaxed microstructures.
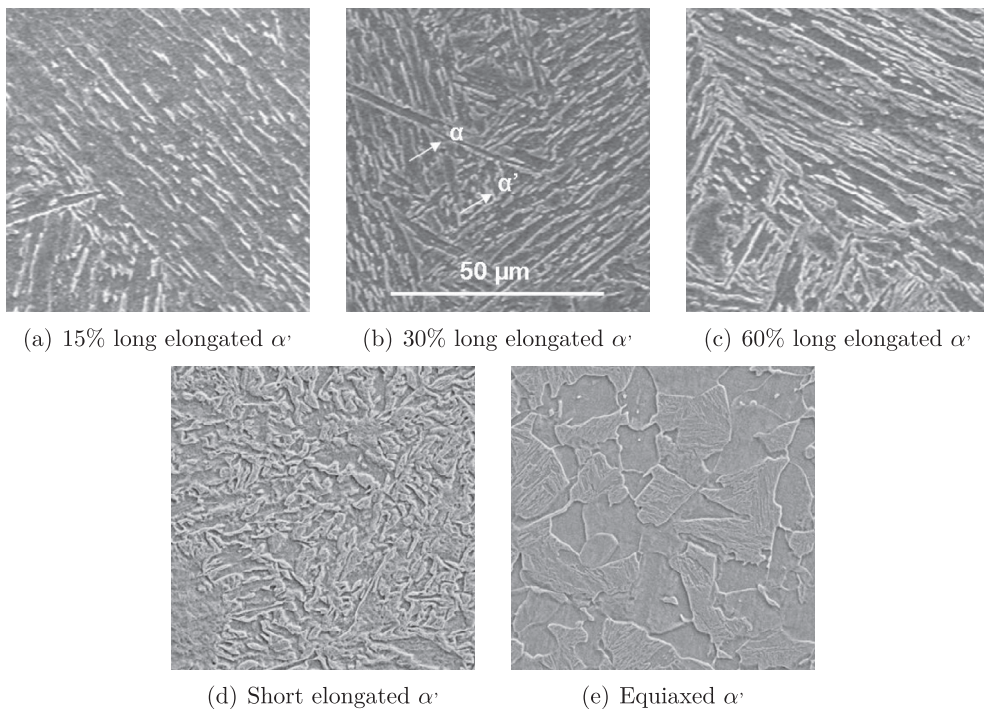

(a) 15% long elongated α' (b) 30% long elongated α' (c) 60% long elongated α'

(d) Short elongated α' (e) Equiaxed α'

Fig. 2. SEM micrographs of the model microstructures (α in dark grey and α' in light grey).

Table 2
Total carbon content of the initial grade and conditions for the second step of the heat treatment to generate the model microstructures with long elongated α'. Actual martensite volume fractions reached after the heat treatment, as measured from SEM micrographs, are also indicated.

$C_{\alpha'}$ [wt.%]	$V_{\alpha'}$ [%]	C_{total} [wt.%]	T [°C]	t [min]	Actual $V_{\alpha'}$ [%]
0.15	15	0.023	720	20	17.2 ± 3.2
0.15	30	0.046	760	20	31.8 ± 1.5
0.15	60	0.088	745	120	59.9 ± 4.3
0.3	15	0.046	735	20	21.0 ± 1.0
0.3	30	0.088	720	600	32.7 ± 5.6
0.3	60	0.175	730	180	58.8 ± 4.8
0.6	15	0.088	702	1380	14.1 ± 3.5
0.6	30	0.175	707	1380	31.1 ± 3.7
0.6	60	0.355	720	600	59.3 ± 2.3

is the principal source of error. Throughout the paper, mentions of carbon content refer to the carbon content within the martensite, $C_{\alpha'}$, unless otherwise indicated.

Three additional model microstructures were considered to highlight the potential influence of the morphology of the α'. Besides the DP steel with (long) Thomas fibres, microstructures with short elongated α' and equiaxed grains were processed by varying the heat-treatment parameters. These additional microstructures contain 60% α' with a C content of 0.15 wt.%. The short fibre microstructure resulted from a decrease in the first holding temperature (Fig. 1(a)) from 1100 to 900 °C. The second step was carried out at 745 °C for 2 h before water quenching to room temperature. As a consequence, the prior

austenite (γ) grain size was reduced to around 20 μm, resulting in shorter martensite fibres in the final microstructure. The microstructure with equiaxed grains was obtained by holding the sample at 900 °C for 5 min and then quenching at 650 °C for 10 s before final water quenching to room temperature (Fig. 1(b)). The time of the second holding was carefully controlled to avoid the formation of pearlite. The size of the α and α' grains is between 20 and 50 μm. Representative micrographs of microstructures with short elongated α' and equiaxed grains are shown in Fig. 2 (d) and (e).

Uniaxial tensile tests were performed at room temperature on 10 mm thick cylindrical dogbone specimens with a gauge length of 100 mm. The tests were carried out at 1 mm min^{-1} using a 50 kN universal mechanical testing machine. Between three and five specimens were tested for each model microstructure. The complete set of experimental results is provided as Supplementary Material to this paper.

2.2. Flow behaviour of dual-phase steels

Fig. 3(a)–(c) presents representative experimental tensile curves for the nine grades of DP steels with long elongated microstructure. The curves are represented up to the onset of necking corresponding to the maximum of the applied force. Only the flow curve for the specimen with 60% α'

with 0.6 wt.% C is represented up to fracture which takes place before the onset of necking in this case. Both the α' volume fraction and C content significantly affect the mechanical response of the DP steels. The 0.2% yield strength increases with the volume fraction of α'. This evolution is linear at fixed C content in the α'. On the other hand, the 0.2% yield strength is almost independent of the C content. The tensile strength, defined as the true stress at maximum load, increases with both α', volume fraction and C content. In contrast, the evolution of the uniform elongation with α' volume fraction and C content is non-monotonous.

Fig. 3(d) presents the experimental tensile curves (up to the onset of necking) for the specimens with 60% α' and 0.15 wt.% C and different α' morphologies. Microstructures with long and short elongated α' exhibit lower yield and tensile strengths than the microstructure with equiaxed α'. The true uniform strain is larger for specimens with long elongated α', compared to short elongated or equiaxed ones.

Fig. 4 presents the evolution of the incremental hardening exponent for varying α' volume fraction and carbon content up to the point of maximum applied force. The incremental hardening exponent is defined as

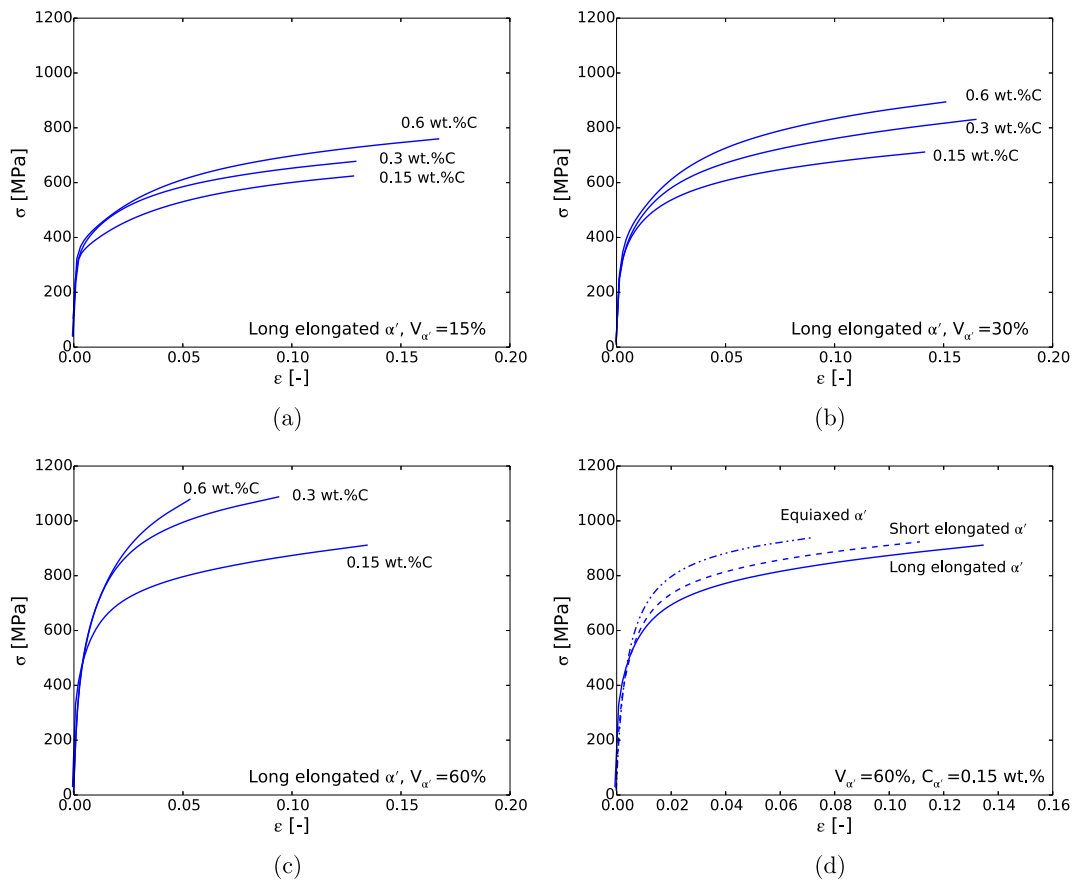$$n_{incr} = \frac{d\sigma}{d\varepsilon} \frac{\varepsilon}{\sigma}. \tag{2}$$

Fig. 3. (a–c) Experimental flow curves up to the onset of necking for various martensite volume fractions and carbon contents (long elongated microstructure). (d) Experimental flow curves up to the onset of necking for various martensite morphologies ($V_{\alpha'} = 60\%$ and $C_{\alpha'} = 0.15$ wt.%).
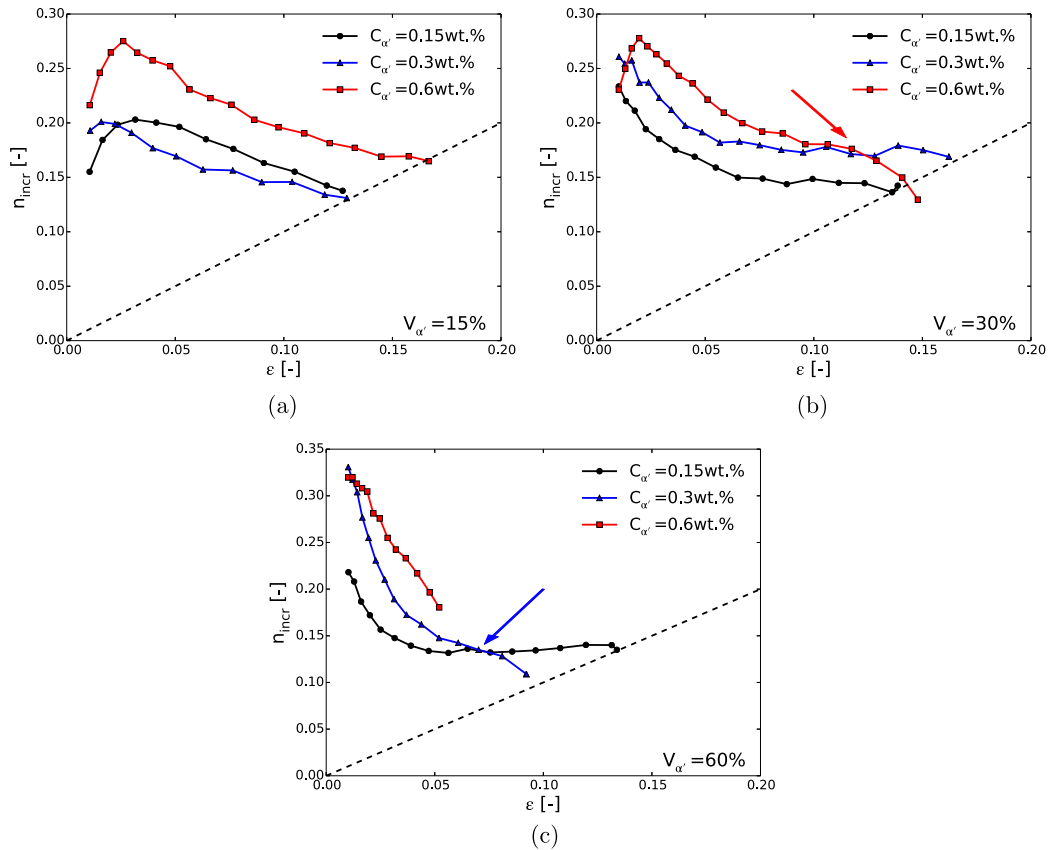
Fig. 4. (a–c) Experimental incremental hardening curves up to the point of maximum load for varying martensite volume fractions and carbon contents (long elongated microstructure). Arrows indicate possible damage-induced softening.

The Considère criterion for the onset of necking can be written: $n_{incr} = \varepsilon$. (This condition holds under the assumption, valid here, that the elastic volume change can be neglected.) All the curves are found to satisfy the Considère criterion at the point of maximum load, except for the samples with 60% α' and 0.6 wt.% C, which break before necking. In general, n_{incr} increases with carbon content in the martensite for a fixed volume fraction. However, the curves corresponding to specimens with $V_{\alpha'} = 30\%$ and $C_{\alpha'} = 0.6$ wt.% on the one hand, and to samples with $V_{\alpha'} = 60\%$ and $C_{\alpha'} = 0.3$ wt.% on the other hand, show a marked decrease in the hardening exponent value at moderate strains, as indicated by an arrow in the figure. This effect can probably be attributed to damage-induced softening which brings about a decrease in the overall ductility. Indeed, damage accumulation can have two effects. Damage can lead to local softening that accelerates the initiation of plastic localization [30]. If damage accumulates fast enough, failure by void coalescence can occur before plastic localization, as observed for the specimens with $V_{\alpha'} = 60\%$ and $C_{\alpha'} = 0.6$ wt.%.

2.3. Flow behaviour of bulk martensite

In order to investigate the role of carbon content on the overall flow behaviour, the tensile response of bulk martensitic samples with various carbon contents was
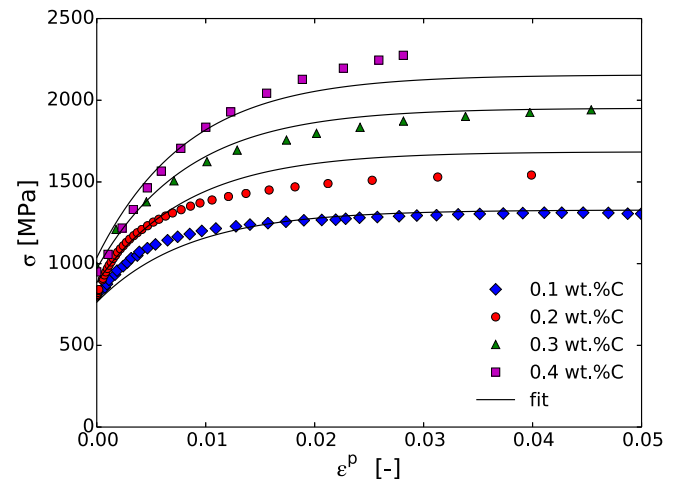

Fig. 5. Tensile behaviour of bulk martensite with varying carbon content. Symbols are the experimental measurements, while the solid line is obtained by fitting the experimental data with the exponential law presented in Section 3.1.

experimentally measured in a former investigation. Specific grades with controlled carbon contents were therefore processed. Four different steels with carbon contents of 0.1, 0.2, 0.3 and 0.4 and 1.5 wt.% were first cast, and then hot- and cold-rolled. Samples were then reheated at 1000°C and water quenched prior to mechanical testing. Fig. 5

shows the flow curve of bulk α' samples. The flow stress and hardening capacity of the martensite increases with increasing carbon content. Experimental data were then fitted with an exponential law to be used in the micromechanical model, as explained in Section 3.1.

3. Modelling

A micromechanical analysis was carried out to further investigate the effect of α' volume fraction and carbon content on the mechanical behaviour of the DP steels. A nonlinear mean-field model was adopted, according to which the overall response of the DP steel is obtained based on an average of the response of the α and α' phases. The partitioning of strain among the phases is determined from simplified interaction laws based on Eshelby's solution. On the other hand, the influence of the carbon content is accounted for at the level of the constitutive response of the α'.

3.1. Constitutive responses of the phases

The constitutive response of each phase is described by classical, rate-independent J_2 elastoplasticity theory with isotropic hardening. The Young's modulus of the α and α' phases is presumed to be identical and set as $E = 210$ GPa and $v = 0.3$.

The flow behaviour of the martensite was fitted based on the experimental flow curves for 100% bulk α' samples in Fig. 5 by using the exponential law

$$\sigma_{y,\alpha'} = \sigma_{y0,\alpha'} + k_{\alpha'}\left(1 - \exp\left(-\varepsilon_p n_{\alpha'}\right)\right) \tag{3}$$

where $\sigma_{y,\alpha'}$ is the current yield strength, ε^p is the accumulated plastic strain, and $\sigma_{y0,\alpha'}, k_{\alpha'}$ and $n_{\alpha'}$ are material parameters. The influence of the carbon content on strain hardening is accounted for in the following way. The initial yield stress, $\sigma_{y0,\alpha'}$ is given by:

$$\sigma_{y0,\alpha'} = 300 + 1000\,C_{\alpha'}^{1/3}, \tag{4}$$

where $C_{\alpha'}$ is the carbon content in the martensite expressed in wt.%. On the other hand, the hardening modulus $k_{\alpha'}$ increases with $C_{\alpha'}$ according to:

$$k_{\alpha'} = \frac{1}{n_{\alpha'}}\left[a + \frac{b\,C_{\alpha'}}{1 + \left(\frac{C_{\alpha'}}{C_0}\right)^q}\right] \tag{5}$$

with $a = 33 \cdot 10^3$ MPa, $b = 36 \cdot 10^4$ MPa, $C_0 = 0.7$ and $q = 1.45$. The hardening exponent is set as $n_{\alpha'} = 120$. Results of the fitting procedure are shown in Fig. 5.

The strain hardening of the ferrite is described by a Swift-type representation:

$$\sigma_{y,\alpha} = \sigma_{y0,\alpha}(1 + H_\alpha \varepsilon^p)^{n_\alpha}, \tag{6}$$

where $\sigma_{y0,\alpha}, H_\alpha$ and n_α are material parameters. These parameters are a priori unknown as they depend on details of the processing route. Hence, they are identified by fitting

the model predictions with a fraction of the experimental data for the DP steels. This set of parameters is kept identical for all the grades of steels considered here.

3.2. Homogenization scheme

The adopted micromechanical model relies on Eshelby's solution for a single, ellipsoidal inclusion in an infinite matrix [31]. Let $\boldsymbol{C}_0$ and $\boldsymbol{C}_1$ be the elastic stiffness of the isolated inclusion and the infinite matrix, respectively. The strain in the isolated inclusion, $\boldsymbol{\varepsilon}_1$, is uniform and related to the far-field strain $\boldsymbol{\varepsilon}_\infty$ by:

$$\boldsymbol{\varepsilon}_1 = \boldsymbol{H}(I, \boldsymbol{C}_0, \boldsymbol{C}_1) : \boldsymbol{\varepsilon}_\infty \tag{7}$$

with

$$\boldsymbol{H}(I, \boldsymbol{C}_0, \boldsymbol{C}_1) = \{\boldsymbol{I} + \boldsymbol{P}(I, \boldsymbol{C}_0) : [\boldsymbol{C}_1 - \boldsymbol{C}_0]\}^{-1} \tag{8}$$

where $\boldsymbol{I}$ is the fourth-order symmetric identity tensor, $\boldsymbol{P}$ is the so-called Hill's polarization tensor and I represents the aspect ratio of the ellipsoidal inclusion. Analytical expressions for $\boldsymbol{P}$ can be found, for instance, in Ref. [32]. In a mean-field model for non-dilute composite, the effect of interacting phases is captured through a suitable choice for the infinite matrix material and the far-field strain to be used in relation (7). In general, the average strain in phase 1 can be related to that in phase 0 by:

$$\boldsymbol{\varepsilon}_1 = \boldsymbol{B} : \boldsymbol{\varepsilon}_0 \tag{9}$$

where $\boldsymbol{B}$ is the strain localization tensor whose expression depends on the chosen mean-field scheme. For a dispersion of inclusions in a continuous matrix, the popular Mori–Tanaka (MT) scheme can be invoked [33]. The strain concentration tensor is then given by:

$$\boldsymbol{B} = \boldsymbol{B}^{MT} = \boldsymbol{H}(I, \boldsymbol{C}_0, \boldsymbol{C}_1). \tag{10}$$

That is, the inclusion phase is treated as a single inclusion isolated in an infinite matrix having the properties of the actual matrix material, and viewing the actual matrix average strain as far-field strain. Alternatively, if the inclusion phase forms a continuous network embedding islands of matrix material, the inverse Mori–Tanaka (IMT) model can be used. The corresponding strain concentration tensor reads:

$$\boldsymbol{B} = \boldsymbol{B}^{IMT} = \{\boldsymbol{H}(I, \boldsymbol{C}_1, \boldsymbol{C}_0)\}^{-1}. \tag{11}$$

Now, the matrix material is treated as a single inclusion embedded in an infinite fictitious matrix having the properties of the actual inclusion phase. In linear elasticity, it can be shown that direct and inverse MT schemes provide respectively lower and upper bounds on the overall stiffness of the composite (for inclusions that are stiffer than the matrix). In Eqs. (10) and (11), the shape and orientation of the isolated inclusion must reflect the symmetry class of the microstructure.

A common assumption when extending mean-field schemes from linear elasticity to elastoplasticity is that

the localization Eq. (9) is still valid provided that increments of strains are used. For the DP steels, we have:

$$\Delta \boldsymbol{\varepsilon}_{\alpha'} = \boldsymbol{B} : \Delta \boldsymbol{\varepsilon}_{\alpha} \qquad (12)$$

which must be solved together with the condition:

$$(1 - V_{\alpha'}) \Delta \boldsymbol{\varepsilon}_{\alpha} + V_{\alpha'} \Delta \boldsymbol{\varepsilon}_{\alpha'} = \Delta \bar{\boldsymbol{\varepsilon}} \qquad (13)$$

where $\Delta \bar{\boldsymbol{\varepsilon}}$ is the prescribed macroscopic strain increment. Following Doghri and Ouaar [34], the reference elastic stiffnesses in Eqs. (10) and (11) are replaced by some isotropic projections of the algorithmic tangent moduli. The latter, as well as the average stress increments for each phase, are obtained from the fully implicit integration of the J_2 theory using the average strain increment of the phase as an input:

$$\Delta \boldsymbol{\sigma}_{\alpha(\alpha')} = \mathcal{F}_{\alpha(\alpha')} \big(\Delta \boldsymbol{\varepsilon}_{\alpha(\alpha')}, \text{(state variables)} \big) \qquad (14)$$

where $\mathcal{F}_{\alpha(\alpha')}$ represents the constitutive model of the α (or the α'), as presented in the previous subsection. Finally, as the α' inclusions are equally distributed in the three directions of space (Fig. 2), conferring on the composite a globally isotropic behaviour, the equivalent inclusion is spherical in the mean-field model. More details about the methodology and numerical implementation of the incremental MT model of elastoplasticity can be found in Ref. [34]. Stress increments are found by averaging over the phases:

$$\Delta \bar{\boldsymbol{\sigma}} = (1 - V_{\alpha'}) \Delta \boldsymbol{\sigma}_{\alpha} + V_{\alpha'} \Delta \boldsymbol{\sigma}_{\alpha'}. \qquad (15)$$

The roles of matrix and inclusion phases in DP steels are not necessarily obvious, given the complexity of the microstructure (Fig. 2). Martensite islands often come into contact with one another, sometimes even surrounding the ferrite grains. Therefore, it is reasonable to assume that the actual behaviour of our DP steels will be intermediate between those predicted by the direct and inverse schemes.

$$\bar{\varepsilon} = \bar{\varepsilon}^{MT} = \bar{\varepsilon}^{IMT}$$
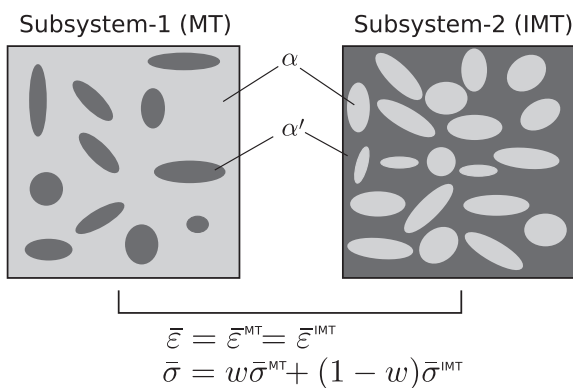$$\bar{\sigma} = w\bar{\sigma}^{MT} + (1 - w)\bar{\sigma}^{IMT}$$

Fig. 6. The mean-field model consists of two subsystems. In the first subsystem, the ferrite is viewed as a continuous matrix reinforced by martensite inclusions, and a direct Mori–Tanaka (MT) scheme is adopted. In the second subsystem, the martensite is viewed as a percolating network surrounding ferrite inclusions, and the inverse Mori–Tanaka (IMT) model is adopted. Each subsystem is subjected to the same macroscopic strain, and the macroscopic stress is computed as the weighted average of the total stress in each subsystem.

Therefore, we considered a modified scheme combining direct and inverse models through an isostrain assumption, as schematically depicted in Fig. (6). The macro-stress is simply computed as the weighted average over the two subsystems:

$$\Delta \bar{\boldsymbol{\sigma}} = w \Delta \bar{\boldsymbol{\sigma}}^{MT} + (1 - w) \Delta \bar{\boldsymbol{\sigma}}^{IMT} \qquad (16)$$

where $w \in [0, 1]$ defines the proportions of direct and inverse contributions to the overall response, and is a fitting parameter. Such a combination of direct MT and IMT models was proposed by Delannay et al. [35] to predict the overall and phase response of DP metals with co-continuous microstructure, and was shown to give very good predictions.

3.3. Parameter identification

The micromechanical model was used to simulate, after proper parameter identification, the uniaxial tensile tests for DP steels with long elongated microstructures. Three different schemes were assessed: the direct scheme ($w = 1$), the inverse scheme ($w = 0$) and a combination of both ($w = 0.5$, following [35]). In each case, the only fitting parameters are the initial yield stress $\sigma_{y0,\alpha}$, hardening modulus H_{α} and exponent n_{α} of the ferrite. These parameters have been determined to obtain the best fit (in a least-squares sense) of the experimental data for the three curves corresponding to $V_{\alpha'} = 15\%$ (Fig. 3(a)). Note that all schemes give identical predictions up to the onset of flow in the ferrite, as the elastic properties of the α and the α' are identical. Subsequent stress and strain partitioning between the phases after yield then drastically differ with the chosen homogenization scheme. Predictions obtained with a direct or an inverse scheme were not satisfactory, as described in the Appendix A.

Results obtained with a combination of direct MT and IMT are presented in Fig. 7 for DP steels with (a) $V_{\alpha'} = 15\%$, (b) $V_{\alpha'} = 30\%$ and (c) $V_{\alpha'} = 60\%$. Numerical predictions are shown up to the onset of necking, as predicted from the Considère criterion: $n_{incr} = \varepsilon$. The optimized ferrite parameters are the following: $\sigma_{y0,\alpha} = 300$ MPa, $H_{\alpha} = 50$ and $n_{\alpha} = 0.33$. The same set of parameters is used for all the α' volume fractions. The model predictions are very satisfying given that only three fitting parameters (in addition to w, but which was fixed from previous investigations [35]) were needed. The model properly captures the effect of the α' volume fraction, as well as that of the carbon content on the composite response.

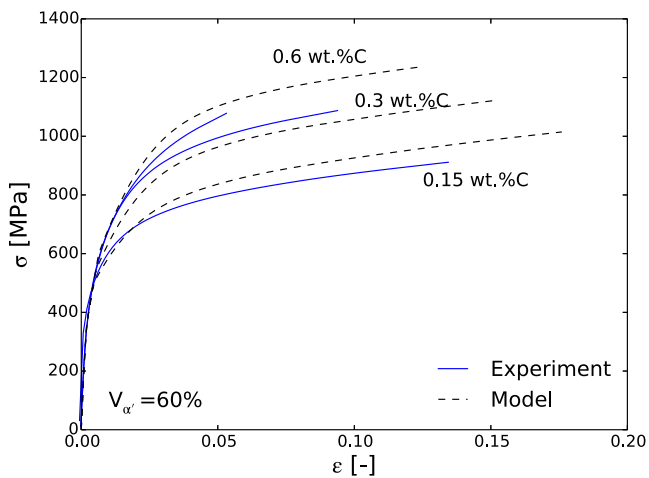### 3.4. Prediction of tensile strength and uniform elongation

Fig. 8 shows the predicted evolutions of the tensile strength σ_u with α' volume fraction, for three carbon contents. Available experimental values and standard deviations are also represented (these data are also given as Supplementary Information). As specimens with
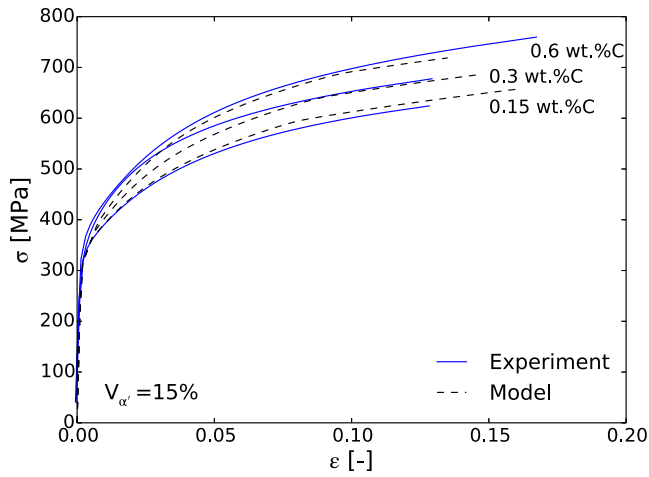
(a)
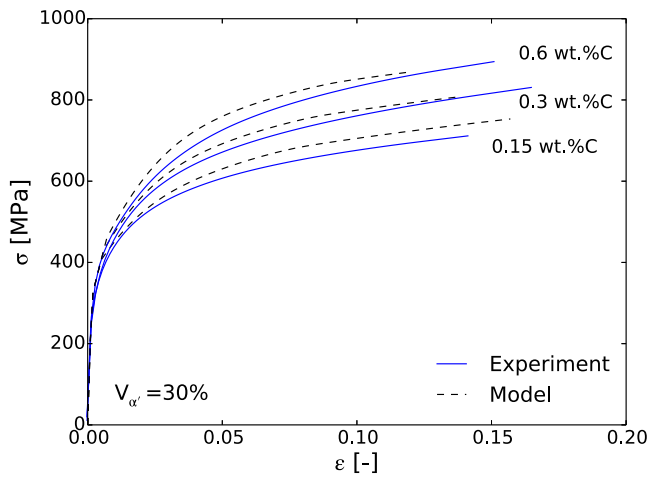
(b)

(c)

Fig. 7. Numerical and experimental flow curves for the DP steels with long elongated microstructures. Flow parameters of the ferrite in the model were fitted on the experimental results for $V_{\alpha'} = 15\%$ only. The same parameters were used to predict the steel responses for $V_{\alpha'} = 30\%$ and $V_{\alpha'} = 60\%$.
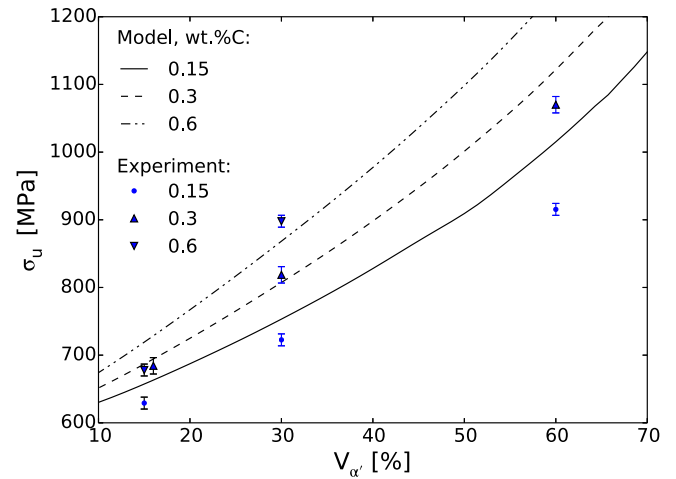
Fig. 8. Evolution of the tensile strength σ_u with the martensite volume fraction for microstructures with long elongated microstructure and varying martensite carbon content.

this grade. Predictions are quite satisfying for the two lowest volume fractions of α', but the model overestimates the tensile strength for $V_{\alpha'} = 60\%$. The model predicts an increase in tensile strength with carbon content at a fixed volume fraction of α', in qualitative agreement with the experimental findings.

Table 3 shows the corresponding predicted evolution of the uniform strain ε_u together with experimental values. The model predicts a non-monotonous evolution of the uniform elongation with an increasing volume fraction of reinforcing phase, with a minimum of ductility reached between $V_{\alpha'} = 30\%$ and $V_{\alpha'} = 50\%$. On the other hand, the model predicts a decrease in ductility with increasing C content for a fixed α' volume fraction. Unfortunately, neither of these trends are supported by experimental data.

Predicting uniform elongation remains a great challenge for the development of microstructure-informed constitutive models. It is intimately connected to an accurate prediction of the strain-hardening response used for each phase convoluted with the additional assumptions associated with the homogenization model. In the present case, the selected models for the α and α' phases (Eqs. (3) and (6)) are certainly good enough to predict the general trends (cf. Fig. 7), but are probably not rich enough to capture minute details of the flow process at large strains. On the other hand, the non-monotonous predictions of the model regarding uniform elongation can be traced back to the adopted averaging procedure based on direct and inverse schemes. Indeed, it can be shown that, considering a direct MT scheme only and using the ferrite properties in Section 3.3, the model predicts an increasing ductility with α' volume fraction in the range $V_{\alpha'} = [0\% - 60\%]$, where plastic flow of α' is insignificant. In contrast, by using the IMT scheme only and still using the ferrite properties in Section 3.3, large plastic deformations of the martensite are predicted, leading to a decreasing ductility with volume fraction associated with a saturation of hardening in the α'.

$V_{\alpha'} = 60\%$ and $C_{\alpha'} = 0.6$ wt.% broke before necking, corresponding tensile strength values could not be obtained for

The overall response is a combination of these two opposite trends within the mean-field model.

4. Discussion

4.1. Influence of the martensite volume fraction

The increase of the flow and tensile strengths with increasing α' volume fraction at fixed carbon content in the α' is well known and widely documented (e.g. [36–38,18], to cite only a few). It is a consequence of the composite effect resulting from the introduction of a large amount of hard particles in a soft phase. Note, however, that the initial yield stress is in principle not altered by the volume fraction of martensite, due to the identical elastic properties of the two phases. The composite effect is qualitatively reproduced by the mean-field model, as expected from such an approach. On the other hand, the impact of the volume fraction of α' on the tensile strength is not necessarily straightforward, as the tensile strength depends also on the uniform strain that can be reached.

In addition to the composite effect, the increase in the α' volume fraction can indirectly influence the response of the α phase in two ways. First, the amount of geometrically necessary dislocations resulting from the martensitic transformation increases. These dislocations are mainly located at the $\alpha - \alpha'$ interface [39,12] and harden the ferrite, as recently confirmed by nanohardness measurements [12,40,13]. Second, the increase of the number and of the size of the α' particles with increasing α' volume fraction induces a decrease in the ferrite mean grain size, d. The ferrite–martensite interfaces constitute impenetrable barriers to dislocations, inducing a strengthening of the α of the Hall–Petch type with increasing flow stress at decreasing d [41,37,19]. By increasing the strength of the α, these two effects in turn increase the hardening of the composite.

The adopted constitutive model for the ferrite does not explicitly account for the strengthening associated with increasing volume fraction of martensite. In principle, these two effects could be introduced at the expense of more elaborate strain-hardening law and additional fitting parameters. For instance, an enriched constitutive model for the ferrite was proposed by Delincé et al. [19] and explicitly accounts for the ferrite grain size (see also Massart and Pardoen [42]). Introducing more complex constitutive models could probably improve the accuracy of the predicted flow curves. Nevertheless, the already satisfactory predictions indicate that these additional effects of α' volume fraction are probably of second order, as compared to the composite effect.

The evolution of uniform elongation with increasing volume fraction of α' for a given carbon content in the α' can be seen from the rows of Table 3. Leaving aside the values of uniform elongations corresponding to specimens in which damage-induced softening or fracture

Table 3
Mean experimental values and numerical predictions of the uniform elongation as a function of the martensite volume fraction and carbon content. Model predictions are indicated in parentheses. An asterisk means that the experimental data are lower than expected as a result of possible early damage-induced softening.

	15% α'	30% α'	60% α'
0.15 wt.% C	0.118	0.119	0.127
(model)	(0.162)	(0.160)	(0.180)
0.3 wt.% C	0.124	0.153	0.08*
(model)	(0.149)	(0.141)	(0.165)
0.6 wt.% C	0.171	0.148*	–
(model)	(0.138)	(0.122)	(0.132)

takes place, our data indicate that the uniform elongation increases with the volume fraction of martensite. This observation seems to contradict the usually reported trend that ductility decreases with increasing volume fraction of martensite (e.g. [18]). However, many previous studies considered only one grade of steel, so that the carbon content and volume fraction of the α' were intrinsically linked (cf. Eq. (1)). In contrast, the present approach allows us to assess the impact of the amount of second phase separately from its carbon content. Referring to Tables 1,2, the evolution of uniform elongation with increasing volume fraction of α' and for a given grade of steel (i.e. for a fixed total carbon content) are found in the diagonals of Table 3. For instance, the main diagonal in Table 3 comprises the results for the DP steels generated from grade 3. Our results indeed indicate a decrease in ductility with volume fraction for a fixed total carbon content.

4.2. Influence of carbon content

Compared to the composite effect, the influence of carbon content has been investigated less systematically in the literature. The present study shows that an increase in the carbon content plays a significant role on the composite behaviour, leading to an increase of the tensile strength of the DP steel. Table 3 also indicates that the uniform elongation increases with carbon content in the martensite for a fixed volume fraction (again, leaving aside samples showing premature necking due to damage-induced softening).

The effect of an increasing $C_{\alpha'}$ is twofold. First, the intrinsic properties of the reinforcing phase change. An increase in the carbon content brings about higher yield strength and extra hardening of the martensite [2,1,43]. This was proved in a previous investigation using nanoindentation measurements in the α' [29], and is also taken into account in the micromechanical model through the flow behaviour of the martensite (see Fig. 5).

Second, the dislocation density at the $\alpha–\alpha'$ interface produced by the transformation of austenite into

martensite increases with increasing carbon content. Indeed, larger carbon content in the γ brings about larger volume changes during the transformation. The experimental results indicate that this effect has little impact on the composite yield stress. Indeed, the initial yielding of the composite is governed by the yielding of the α phase. In the latter, plastic deformation occurs first at the centre of the grain where the phase is softer and the dislocations located at the interface do not affect the onset of yielding. However, the presence of the dislocations in regions near the α–α' interfaces leads to an increase of the work-hardening rate. This latter effect of carbon content was not incorporated into the micromechanical model. However, the reasonable agreement between model and experimental results suggests that the effect of carbon on the ferrite response is less important than that of carbon on the martensite response.

4.3. Influence of the morphology of the α'

The specimen with large equiaxed α' particles presents a larger yield and tensile strength compared to microstructures with elongated α' islands where particles are more finely dispersed in the α phase (Fig. 3(d)). A similar result has been reported by Kim and Thomas [3] and He et al. [44], who showed that a coarse microstructure induces a larger tensile strength when compared to finely dispersed α' islands. The morphology and distribution of the α' influence the load transfer between the two phases [45,18]. The presence of α' islands at the grain boundaries, as encountered in equiaxed microstructures (Fig. 2(e)), restricts the plastic flow in the α phase and increases the yield stress. In addition, the percolating network of α' increases the portion of load carried by the martensite phase, as compared to specimens with finely dispersed α' particles. The higher strength and lower ductility observed in specimens with equiaxed microstructure could therefore be explained by an earlier onset of damage by void nucleation or fracture of the α' inclusions, due to higher stress levels in the martensite.

In its present state, the adopted mean-field model cannot capture the effect of morphology on the macroscopic response, as it makes no formal distinction between equiaxed, short and long elongated microstructures. Indeed, the only microstructure parameters of the model are the volume fraction of second phase and the global symmetry of the system (through the shape of the equivalent inclusion). The only way such a model could differentiate the response for different morphologies is through the response of the phases, and/or the choice of scheme. For instance, one could consider a refined ferrite hardening model which accounts on additional physical parameters such as the mean-free path or the grain size, which vary within the considered morphologies. The relative weights of the direct MT and IMT schemes could also be adapted to account for varying degrees of percolation. We leave this possible path of investigation for future work.

4.4. Fracture: preliminary considerations

The homogenization model provides predictions of the average phase response within the DP steel. These predictions can also be exploited to gain further insight into the fracture behaviour of the steel. The assumption of premature necking due to softening-induced damage in some of the samples can also be assessed. In a simple approach, fracture is assumed to take place once the maximum principal stress in the α' reaches a critical value, $\sigma_{c,\alpha'}$. This criterion represents the onset of void nucleation in between adjacent martensite grains or by decohesion at α–α' interfaces, which are the dominant damage mechanisms in DP steels [46]. It also assumes that the damage process would be dominated by void nucleation more than by void growth, with void coalescence occurring quickly after
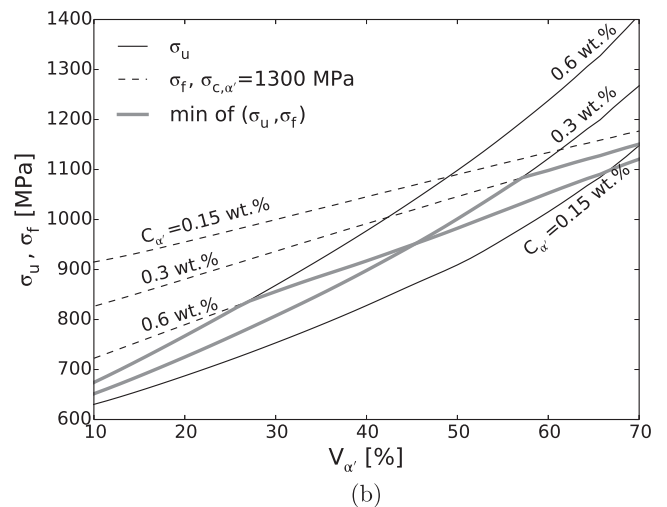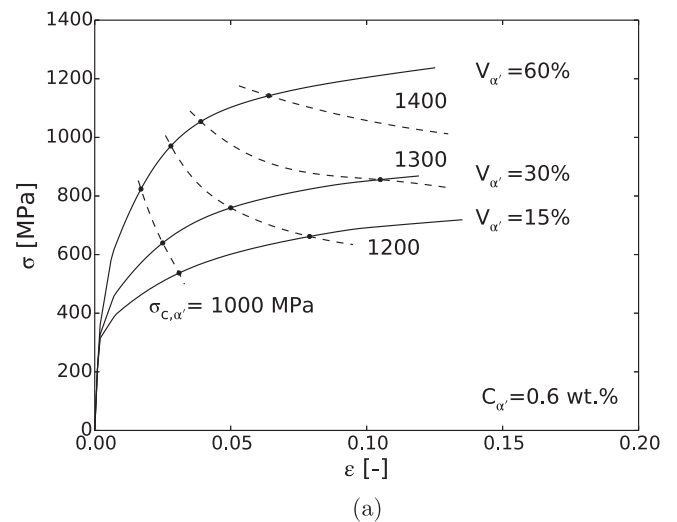

Fig. 9. (a) Locus of fracture, as predicted by a maximum principal stress criterion in the martensite, for varying values of the martensite critical stress $\sigma_{c,\alpha'}$. (b) Evolution of the tensile strength σ_u (black solid lines) and the fracture strength σ_f (dashed lines) with the volume fraction of martensite $V_{\alpha'}$. Grey lines indicate the maximum reachable stress.

nucleation. This view is increasingly valid when the volume fraction of α′ is large.

Fig. 9(a) shows the numerical stress–strain curves for $C_{\alpha'} = 0.6$ wt.% up to the onset of necking. Dashed lines represent the locus of the onset of damage, for varying values of the critical stress $\sigma_{c,\alpha'}$ taken within a realistic range [47]. (Intersections between dashed and solid lines are actual numerical predictions, while the dashed line is a visual guide.) Corresponding experimental results indicate that the grade with $V_{\alpha'} = 60\%$ breaks before necking. In Fig. 3(c), the fracture strain is $\varepsilon = 5.3\%$ (the average fracture strain over five tests is $\varepsilon = 3.2\%$). This trend is reasonably captured by the model, assuming the value $\sigma_{c,\alpha'} \approx 1300$ MPa. A value of 1300 MPa is not far from the critical stress for nucleation of 1200 MPA estimated by Landron et al. [47]. On the other hand, this simple model predicts that necking occurs first for the grades with $V_{\alpha'} = 15\%$ and $V_{\alpha'} = 30\%$. However, the stress level in the martensite for the grades with $V_{\alpha'} = 30\%$ at the point of uniform elongation is of the order of the critical value for the onset of damage, thus supporting our assumption of damage-induced softening for those grades.

This simple approach to fracture is now extended to a broader range of $C_{\alpha'}$ and volume fractions. Fig. 9(b) superimposes the evolutions with $V_{\alpha'}$ of tensile strengths σ_u (black solid lines, previously presented in Fig. 8) and fracture stresses σ_f (dashed lines). The fracture stress σ_f is here defined as the macroscopic stress dictated by the attainment of $\sigma_{c,\alpha'}$ in the α′. The critical stress is set as $\sigma_{c,\alpha'} = 1300$ MPa. The figure indicates that, for a given C content in the α′, damage is due to necking below some value of $V_{\alpha'}$. Above this value, local damage occurs prior to necking (see the grey solid lines in the figure). The transition value of $V_{\alpha'}$ between necking-dominated and fracture-dominated behaviours decreases with increasing $C_{\alpha'}$.

These preliminary results illustrate the potential of micromechanical models as a guide towards microstructure optimization. With this final goal in mind, model
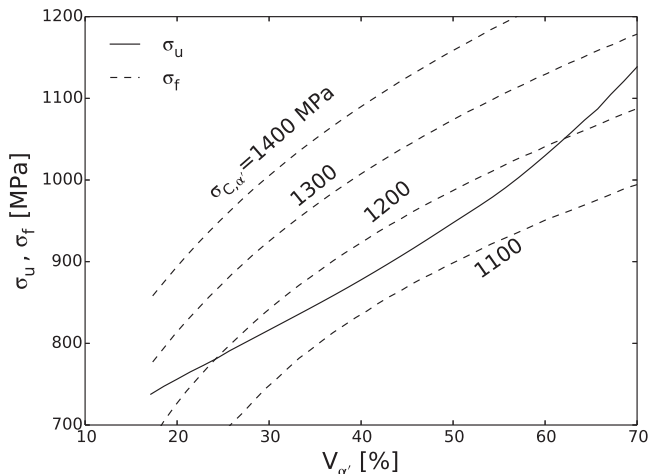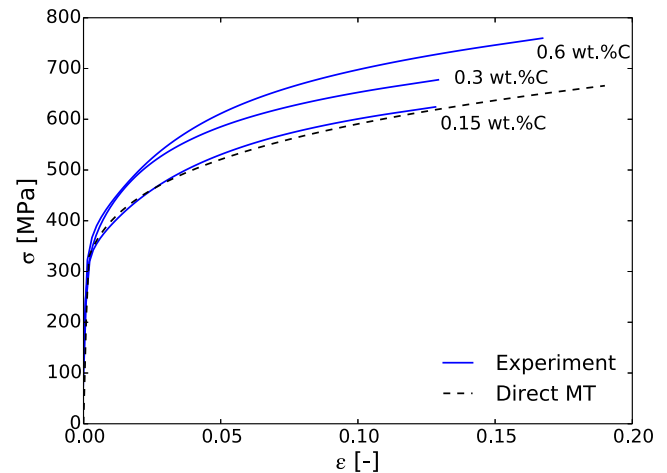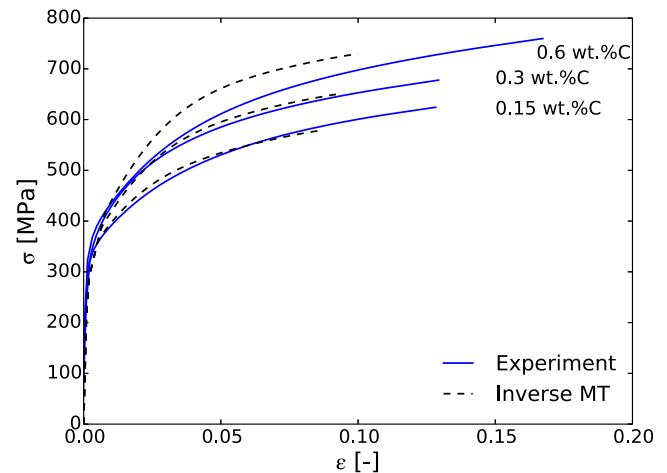

(a) $C_{\text{total}} = 0.1$ wt.%
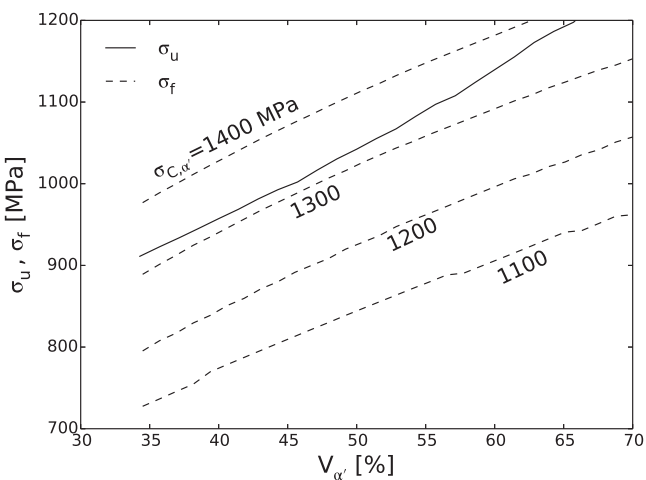
(b) $C_{\text{total}} = 0.2$ wt.%

Fig. 10. Evolution of the tensile strength σ_u (black solid line) and fracture strengths σ_f (dashed lines) with the volume fraction of martensite $V_{\alpha'}$, for varying martensite critical stress $\sigma_{c,\alpha'}$.

(a)

(b)

Fig. 11. Model predictions obtained with (a) the direct Mori–Tanaka scheme and (b) the inverse Mori–Tanaka scheme for $V_{\alpha'} = 15\%$. In each case the ferrite hardening parameters were fitted to obtain the best prediction in a least-squares sense.

predictions are better represented in terms of fixed *total* carbon content, C_{total} which is the parameter that is varied in practice. Fig. 10(a) and (b) present the evolution with $V_{\alpha'}$ of the tensile strength and fracture stress for two fixed values of C_{total}. The carbon content within the martensite now varies with the volume fraction according to Eq. (1). Numerical predictions are shown up to $C_{\alpha'} = 0.6$ wt.%. Still assuming that $\sigma_{c,\alpha'} = 1300$ MPa, the model predicts that grades with $C_{total} = 0.1$ wt.% do not break before necking, while those with $C_{total} = 0.2$ do.

The validity of model predictions depends upon the accuracy of the micromechanical model in predicting the phase response. Moreover, fracture is triggered by discrete events whose occurrence depends on local values of the stress field. By construction, local values of fields are not available from the adopted micromechanical model. Therefore, extensive experimental validations are needed to confirm the predictive capabilities of the model. On the other hand, the failure criterion introduced here is extremely simple. The impact of the change of constraint in the α when changing the α' volume fraction will play a role in modifying the void growth rate due to changes in stress triaxiality [48]. Also, changing $V_{\alpha'}$ modifies the relative spacing between voids, affecting the onset of void coalescence (e.g. [49]). More advanced damage models should consider also the void growth and coalescence stages to obtain more quantitative predictions as in Ref. [47].

5. Conclusion

This paper presents an experimental study of the flow properties of DP steels by varying systematically and independently three microscopic parameters: the martensite volume fraction, its carbon content and the microstructure morphology. In addition, a non-linear micromechanical model was implemented, which explicitly accounts for the effects of the martensite volume fraction and carbon content on the steel response. Numerical predictions from homogenization theory are in good qualitative agreement with experimental stress–strain curves, the only fitting parameters being the flow parameters for the ferrite. The model provides additional insight into the dominant deformation mechanisms. It is also worth pointing out the extremely low computational cost of the approach, as compared to full-field finite-element simulations on representative microstructures, which is key for future extensive modelling-informed microstructure optimization.

The influence of the three microscopic parameters are summarized as follows:

- The increase of the martensite volume fraction results in larger yields and tensile strengths of the DP steels. These trends stem mostly from the composite effect due to the presence of hard particles in a soft matrix. The possible effects of the martensite volume fraction on the ferrite hardening seem to affect the overall response to a lesser extent, as suggested by the micromechanical model.

- The increase in carbon content increases the hardening and tensile strength of the DP steels, but does not affect the initial yield point. This effect can be explained to a large extent by the effect of carbon on the flow response of the martensite. Good predictions can be obtained from the micromechanical model by introducing the martensite constitutive response as determined from bulk martensite samples with varying carbon contents.

- The ductility in general increases with the volume fraction of martensite at constant martensitic carbon content, and conversely increases with the martensitic carbon content at a fixed volume fraction of martensite. Departure from the general trend is observed for combinations of large volume fraction of martensite with large martensitic carbon content, and is attributed to damage-induced softening or fracture.

- The morphology significantly impacts the mechanical behaviour at a given composition and volume fraction. Equiaxed microstructures present higher strength and lower ductility, as compared to specimens with finely dispersed elongated particles. The plastic flow of the ferrite is more constrained in equiaxed microstructures, due to martensite particles acting as a continuous network along grain boundaries.

Acknowledgements

Appendix A. Model predictions with direct and inverse schemes

Fig. 11(a) shows the predictions obtained with the direct MT scheme ($w = 1$). The flow parameters of the ferrite are the following: $\sigma_{y0,\alpha} = 315$ MPa, $H_\alpha = 290$ and $n_\alpha = 0.18$, as the best fit for the experimental curves with $V_{\alpha'} = 15\%$. The direct scheme gives an identical response of the DP steels for all the considered C contents. Indeed, the direct scheme predicts a purely elastic response of the martensite, while in our model carbon affects the response of DP steels only through the plastic flow of the α'. The purely elastic response of the α' results from the weak load transfer from the soft matrix to the hard inclusion. Increments of overall deformation are mainly accommodated by the ferrite, preventing sufficient strain and stress build-up in the martensite to cause flow. Delincé et al. [19] made a similar observation, adopting a secant version of the direct MT scheme. In addition, the direct scheme overestimates the uniform elongation, the latter being close to that of the unreinforced ferrite (as predicted from the Considère criterion, $\varepsilon_u = n_\alpha = 0.18$).

The weak load transfer was previously investigated by comparing direct scheme predictions to reference, finite-element predictions obtained on "ideal" microstructures (a random dispersion of ellipsoids in a continuous matrix) [50,51]. It was found that the incremental Mori–Tanaka scheme strongly underestimates the stress build-up within the inclusions. This known shortcoming of the direct scheme in predicting the response of elastoplastic composites constitutes an additional motivation for considering a combination of direct and inverse schemes.

The best predictions obtained with an IMT scheme ($w = 0$) are shown in Fig. 11(b). The fitting parameters are now: $\sigma_{y0,\alpha} = 270$ MPa, $H_\alpha = 27$ and $n_\alpha = 0.34$. In this case plastic flow of the α' is predicted shortly after that of the ferrite, producing markedly different responses depending on the carbon content. This follows from the treatment of the martensite phase as a continuous matrix subjected to the overall strain. While the model gives good predictions of the overall response for the two lower carbon contents, it markedly overestimates the stress in the 0.6 wt.% C case. In addition, the inverse model strongly underestimates the ductility as a result of the early hardening saturation in the martensite (Fig. 5).

Appendix B. Supplementary data

Supplementary data associated with this article can be found, in the online version, at http://dx.doi.org/10.1016/j.actamat.2014.04.015.

References

[1] G. Speich, R. Miller, Mechanical properties of ferrite-martensite steels, In: Structure and Properties of Dual-Phase Steels, 1979, p. 145–182.

[2] Davies R. Influence of martensite composition and content on the properties of Dual-Phase steel. Metall Trans A 1978;9:671–9.

[3] Kim N, Thomas G. Effect of morphology on the mechanical behavior of a Dual-Phase Fe/2Si/0.1C steel. Metall Trans 1981;12A:483–9.

[4] Marder A. Deformation characteristics of Dual-Phase steels. Metall Mater Trans A 1982;13(1):85–92.

[5] Chen H-C, Cheng G-H. Effect of martensite strength on tensile strength of Dual-Phase steels. J Mater Sci 1989;24:1991–4.

[6] Tomita Y. Effect of morphology of second-phase martensite on tensile properties of Fe-0.1C Dual-Phase steels. J Mater Sci 1990;25:5179–84.

[7] Cong Z, Jia N, Sun X, Ren Y, Almer J, Wang Y. Stress and strain partitioning of ferrite and martensite during deformation. Metall Mater Trans A 2009;40(6):1383–7.

[8] Sun X, Choi K, Liu W, Khaleel M. Predicting failure modes and ductility of Dual-Phase steels using plastic strain localization. Int J Plast 2009;25:1888–909.

[9] Jacques P, Furnémont Q, Godet S, Pardoen T, Conlon K, Delannay F. Micromechanical characterisation or TRIP-assisted multiphase steels by in-situ neutron diffraction. Philos Mag A 2006;86:2371–92.

[10] Woo W, Em V, Kim E-Y, Han S, Han Y, Choi S. Stress-strain relationship between ferrite and martensite in a dual-phase steel studied by in situ neutron diffraction and crystal plasticity theories. Acta Mater 2012;60:6972–81.

[11] Delince M, Jacques P, Pardoen T. Separation of size-dependent strengthening contributions in fine-grained Dual-Phase steels by nanoindentation. Acta Mater 2006;54:3395–404.

[12] Kadkhodapour J, Raabe SSD, Ziaei-Rad S, Weber U, Calcagnotto M. Experimental and numerical study on geometrically necessary dislocations and non-homogeneous mechanical properties of the ferrite in a Dual-Phase steels. Acta Mater 2011;59:4387–94.

[13] Ghassemi-Armaki H, Maaß R, Bhat S, Sriram S, Greer J, Kumar K. Deformation response of ferrite and martensite in a dual-phase steel. Acta Mater 2014;62:197–211.

[14] Stewart J, Jiang L, Williams J, Chawla N. Prediction of bulk tensile behavior of dual-phase stainless steels using constituent behavior from micropillar compression experiments. Mater Sci Eng A 2012;534:220–7.

[15] Kuang S, Kang Y-L, Yu H, Liu R-D. Stress-strain partitioning analysis of constituent phases in dual phase steel based on the modified law of mixture. Int J Miner Metall Mater 2009;16:393–8.

[16] Paul S, Mukherjee M. Determination of bulk flow properties of a material from the flow properties of its constituent phases. Comput Mater Sci 2014;84:1–12.

[17] Berbenni S, Favier V, Lemoine X, Berveiller M. Micromechanical modeling of the elasto-viscoplastic behavior of polycrystalline steels having different microstructures. Mater Sci Eng A 2004;372:128–36.

[18] Mazinani M, Poole W. Effect of martensite plasticity on the deformation behavior of a low-carbon Dual-Phase steel. Metall Mater Trans A 2007;38:328–39.

[19] Delincé M, Bréchet Y, Embury J, Geers M, Jacques P, Pardoen T. Structure property optimization of ultrafine-grained Dual-Phase steels using a microstructure-based strain hardening model. Acta Mater 2007;55:2337–50.

[20] Brassart L, Doghri I, Delannay L. Self-consistent modeling of DP steel incorporating short range interactions. Int J Mater Form 2009;2:447–50.

[21] Delannay L, Pierman A-P, Jacques P. Assessment of a micro-macro modeling of the bending and unbending of multiphase steel sheets. Adv Eng Mater 2009;11:148–52.

[22] Choi K, Liu W, Sun X, Khaleel M. Influence of martensite mechanical properties on failure mode and ductility of Dual-Phase steels. Metall Mater Trans A 2009;40:796–809.

[23] Uthaisangsuk V, Prahl U, Bleck W. Modelling of damage and failure in multiphase high strength DP and TRIP steels. Eng Fract Mech 2011;78:469–86.

[24] Kadkhodapour J, Butz A, Ziaei-Rad S, Schmauder S. A micromechanical study of failure initiation of dual phase steels under tension using single crytal plasticity model. Int J Plast 2011;27:1103–25.

[25] Paul S, Kumar A. Micromechanics based modeling to predict flow behavior and plastic strain localization of dual phase steels. Comput Mater Sci 2012;63:66–74.

[26] Kim E-Y, Yang H, Han S, Kwak J, Choi S-H. Effect of initial microstructure on strain-stress partitioning and void formation in DP980 steel during uniaxial tension. Metal Mater Int 2012;18:573–82.

[27] Marvi-Mashadi M, Mazinani M, Rezaee-Bazzaz A. FEM modeling of the flow curves and failure modes of dual phase steels with different martensite volume fractions using actual microstructures as the representative volume. Comput Mater Sci 2012;65:197–202.

[28] Chen P, Ghassemi-Armaki H, Kumar S, Bower A, Bhat S, Sadagopan S. Microscale-calibrated modeling of the deformation response of dual-phase steels. Acta Mater 2014;65:133–49.

[29] A.-P. Pierman, Micromechanical study of the influence of the microstructure and composition on the plastic flow and damage properties of Dual-Phase steels, [Ph.D. thesis]. Université catholique de Louvain (2013). URL: http://hdl.handle.net/2078.1/129072.

[30] Needleman A, Rice J. Limits to ductility set by plastic flow localization. In: Koistinen D, Wang N, editors. Mechanics of Sheet Metal Forming. Plenum Press; 1978. p. 237–67.

[31] Eshelby JD. The determination of the elastic field of an ellipsoidal inclusion, and related problems. Proc R Soc London A 1957;241:376–96.

[32] Walpole L. Elastic behavior of composite materials: theoretical foundations. Adv Appl Mech 1981;21:169–203.

[33] Mori T, Tanaka K. Average stress in matrix and average elastic energy of materials with misfitting inclusions. Acta Metall 1973;21:571–4.

[34] Doghri I, Ouaar A. Homogenization of two-phase elasto-plastic composite materials and structures: study of tangent operators, cyclic plasticity and numerical algorithms. Int J Solids Struct 2003;40:1681–712.

[35] Delannay L, Lani F, Pardoen T, Delannay F. Mean field modelling of the plastic behaviour of co-continuous Dual-Phase alloys with strong morphological anisotropy. Int J Plast 2006;22:2327–45.

[36] Byun T, Kim I. Tensile properties and inhomogeneous deformation of ferrite–martensite dual-phase steels. J Mater Sci 1993;28: 2923–32.

[37] Jiang Z, Guan Z, Lian J. Effects of microstructural variables on the deformation behaviour of dual-phase steel. Mater Sci Eng A 1995;190:55–64.

[38] Bag A, Ray K, Dwarakadasa E. Influence of martensite content and morphology on tensile and impact properties of high-martensite dual-phase steel. Metall Mater Trans A 1999;30A:1193–202.

[39] Jacques P, Furnémont Q, Mertens A, Delannay F. On the sources of work hardening in multiphase steels assisted by transformation-induced plasticity. Philos Mag A 2001;81:1789–812.

[40] Tsipouridis P, Koll L, Krempaszky C, Werner E. On the strength of grain and phase boundaries in ferritic-martensitic dual-phase steels. Int J Mater Res 2011;102:674–86.

[41] Chang P-H, Prebann A. The effect of ferrite grain size and martensite volume fraction on the tensile properties of dual-phase steels. Acta Metall 1985;5:897–903.

[42] Massart T, Pardoen T. Strain gradient plasticity analysis of the grain-size-dependent strength and ductility of polycrystals with evolving grain boundary confinement. Acta Mater 2010;58:5768–81.

[43] Chen H, Era H, Shimizu M. Effect of phosphorus on the formation of retained austenite and mechanical properties in Si-containing low-carbon steel sheet. Metall Trans A 1989;20A:437–45.

[44] He X, Terao N, Berghezan A. Influence of martensite morphology and its dispersion on mechanical properties and fracture mechanisms of Fe-Mn-C Dual-Phase steels. Metal Sci 1984;18:367–73.

[45] Sarwar M, Priestner R. Influence of ferrite-martensite microstructural morphology on tensile properties of dual-phase steel. J Mater Sci 1996;31:2091–5.

[46] Lacroix G, Pardoen T, Jacques P. The fracture toughness of TRIP-assisted multiphase steels. Acta Mater 2008;56:3900–13.

[47] Landron C, Bouaziz O, Maire E, Adrien J. Characterization and modeling of void nucleation by interface decohesion in dual-phase steels. Scr Mater 2010;63:973–6.

[48] Yerra S, Martin G, Véron M, Bréchet Y, Mithieux J, Delannay L, et al. Ductile fracture initiated by interface nucleation in two-phase elastoplastic systems. Eng Fract Mech 2013;102:77–100.

[49] Tekoglu C, Pardoen T. A micromechanics based damage model for composite materials. Int J Plast 2010;26:549569.

[50] Delannay L, Doghri I, Pierard O. Prediction of tension-compression cycles in multiphase steel using a modified incremental mean-field model. Int J Solids Struct 2007;44:7291–306.

[51] Brassart L, Doghri I, Delannay L. Homogenization of elasto-plastic composites coupled with a nonlinear finite element analysis of the equivalent inclusion problem. Int J Solids Struct 2010;47:716–29.